A normal mode stability analysis of numerical interface conditions for fluid/structure interaction

J. W. Banks[1,*], B. Sjögreen[1]

[1] *Center for Applied Scientific Computing, Lawrence Livermore National Laboratory, Livermore, California, 94551*

Abstract. In multi physics computations where a compressible fluid is coupled with a linearly elastic solid, it is standard to enforce continuity of the normal velocities and of the normal stresses at the interface between the fluid and the solid. In a numerical scheme, there are many ways that velocity- and stress-continuity can be enforced in the discrete approximation. This paper performs a normal mode stability analysis of the linearized problem to investigate the stability of different numerical interface conditions for a model problem approximated by upwind type finite difference schemes. The analysis shows that depending on the ratio of densities between the solid and the fluid, some numerical interface conditions are stable up to the maximal CFL-limit, while other numerical interface conditions suffer from a severe reduction of the stable CFL-limit. The paper also presents a new interface condition, obtained as a simplified charcteristic boundary condition, that is proved to not suffer from any reduction of the stable CFL-limit. Numerical experiments in one space dimension show that the new interface condition is stable also for computations with the non-linear Euler equations of compressible fluid flow coupled with a linearly elastic solid.

AMS subject classifications: 65M12, 35L60, 35L65

Key words: Finite difference method, Normal mode analysis, Fluid/structure interaction, Compressible fluid, Interface condition

1 Introduction

The subject of this article is the stability of numerical approximations of fluid-structure interaction problems with particular emphasis on high-speed flow applications. This type of fluid-structure interaction occurs in many application areas including aeroelasticity, modeling of explosives, and others. Numerous previous works have developed numerical methods for this type of problem (for example [1, 2]).

Although many large scale computations of fluid-structure interaction have been performed to date, see, e.g., [3,4], the theory of stability and convergence of numerical schemes

*Corresponding author. *Email addresses:* banks20@llnl.gov, sjogreen2@llnl.gov

for such problems is less developed. The aim of this paper is to improve the understanding of the underlying mathematical properties of approximations for fluid-structure interaction problems, and thereby facilitate improvements in accuracy and efficiency of the numerical methods.

We introduce a one dimensional linear problem, obtained by linearizing the equations of inviscid compressible fluid flow coupled with a linear elasticity model. This simple model, which consists of two coupled wave equations, gives insight into the different numerical behaviors that occur at the interface between the materials. It turns out that for explicit time stepping schemes, one critical parameter affecting the numerical stability is the ratio of the densities on either side of the interface.

For problems in aeroelasticity, the density of the solid material is usually several orders of magnitude larger than the density of the fluid. However, in other fluid-structure interaction applications, such as explosives modeling, the density ratio can be very close to one. Although standard numerical methods often can be tuned to a specific density ratio, a coupling method that performs well regardless of the density ratio between the solid and fluid would be more convenient. This is especially true for non-linear problems where the density ratio can vary widely from point to point along the interface and also in time.

One remedy for instabilities is to switch to implicit coupling. However, when the objective is to resolve all time scales (as if often the case in high-speed compressible applications), explicit methods are preferable because of their lower computational cost. This paper shows that by chosing appropriate numerical interface conditions it is possible to have a stable explicit method for any density ratio, that does not suffer from any CFL restriction other than that of the numerical schemes in the respecive solid and fluid parts of the domain.

Section 2 introduces a one dimensional fluid-structure example problem, where a few standard methods with explicit time stepping are shown to be stable or unstable depending on the density ratio. A simplified model problem is then derived via linearization. The explanation for the unstable behavior is captured in the analysis of the model problem presented in Section 3. Section 3 also introduces a new numerical interface condition that is proved to be stable with explicit time stepping for any density ratio. Numerical experiments with the model problem in Section 4 compare the performance of the different interface conditions, confirming the analytical results. Finally, in Section 4.1, the generalization of the new stable interface condition to the fluid/structure example from Section 2, shows stable behavior in numerical experiments with both small and large density ratios.

2 Introductory example

A fluid, described by the inviscid Euler equations of compressible gas dynamics, interacts with an elastic body, described by the equations of structural mechanics for a linearly elastic material. Assume a one-dimensional problem with a single interface between the

solid and the fluid located at $x=x_I(t)$. The fluid domain is $x>x_I(t)$ and the solid domain is $x<x_I(t)$. The equations of the model in the Lagrangian (material) coordinate X are

$$\begin{bmatrix} \rho \\ \rho u \\ e \end{bmatrix}_t + \begin{bmatrix} \rho u - \rho s \\ \rho u^2 + p - \rho u s \\ u(e+p) - e s \end{bmatrix}_X = \begin{bmatrix} 0 \\ 0 \\ 0 \end{bmatrix} \quad X>0 \tag{2.1}$$

$$\begin{bmatrix} u \\ \sigma \\ x \end{bmatrix}_t + \begin{bmatrix} -\frac{1}{\rho^{(s)}}\sigma \\ -Eu \\ 0 \end{bmatrix}_X = \begin{bmatrix} 0 \\ 0 \\ u \end{bmatrix} \quad X<0. \tag{2.2}$$

The unknowns are functions of the Lagrangian coordinate X, and time t. The Eulerian (physical) coordinate is a function $x=x(X,t)$ that traces the material points, defined such that $x(X,0)=X$. The interface location in the Eulerian coordinate is $x_I(t)=x(0,t)$. The density of the solid is given by $\rho(X,t)=\rho^{(s)}/x_X(X,t)$, where the initial density is assumed to be the constant $\rho^{(s)}$. E is the constant Young's modulus. The fluid equations are formulated in a rigid coordinate system that moves with the velocity of the interface, $s=s(t)=dx_I(t)/dt$. This is a natural extension of the Lagrangian coordinate to the fluid domain. The dependent variables in the fluid are the density, ρ, the velocity u, and the total energy e. The pressure is given by the gamma law equation of state $p=(\gamma-1)(e-\frac{1}{2}\rho u^2)$, where $\gamma=1.4$. The dependent variables in the solid are the velocity u, the stress σ, and the coordinate x. Superscripts will indicate whether a variable belongs to the fluid or to the solid, e.g., $u^{(s)}$ is the velocity in the solid and $u^{(f)}$ is the velocity in the fluid. Superscripts will be omitted when it is clear from the context if a variable belongs to the fluid or to the solid.

At a continuous level, the interface conditions are continuity of velocity and stress

$$u^{(s)}(0,t)=u^{(f)}(0,t) \tag{2.3}$$

$$\sigma(0,t)=-p(0,t). \tag{2.4}$$

The numerical approximation of the fluid/structure system (2.1), (2.2) is done on a computational domain $[-1,1]$ with the grid $X_i^{(s)}=\Delta x(i-1/2)$, $i=-N,-N+1,\ldots,0$ for the solid, and $X_i^{(f)}=\Delta x(i+1/2)$, $i=0,1,\ldots,N$ for the fluid. The grid points $X_1^{(s)}$ and $X_{-1}^{(f)}$ are ghost points that faciliate imposing the interface condition. The number of grid points in each domain $N-1$, and the grid spacing Δx, are related by $1=\Delta x(N-1)$. The interface is located between the last point in the solid and the first point in the fluid, $X_0^{(s)}=-\Delta x/2$ and $X_0^{(f)}=\Delta x/2$ respectively. This computational setup is shown schematically in Figure 1.

A dependent variable, $q(X,t)$, approximated at time level $t_n=n\Delta t$ and grid point i is denoted q_i^n. In the description of the interface conditions below, the time superscript n will often be left out. The equations (2.1) and (2.2) are approximated by the Godunov scheme (see [5] for example). Equation (2.2) is a linear hyperbolic problem, and the Godunov scheme is identical to the upwind scheme. The numerical schemes are explicit three point schemes, and thus advance the solution from time t_n to t_{n+1} at all points

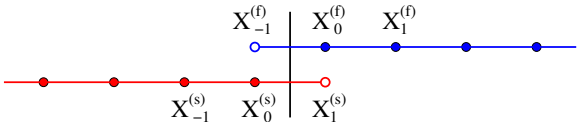

Figure 1: Schematic of the solid (left) and fluid (right) grids for the model fluid structure discretization.

except at the ghost points $X_1^{(s)}$ and $X_{-1}^{(f)}$. Extrapolation with first order accuracy gives the density of the fluid at the ghost point, $(\rho^{(f)})_{-1}^{n+1} = (\rho^{(f)})_0^{n+1}$. Updates to the Eulerian coordinates are defined in the solid by $(x^{(s)})_i^{n+1} = (x^{(s)})_i^n + \Delta t (u^{(s)})_i^n$, and in the fluid as $(x^{(f)})_i^{n+1} = (x^{(f)})_i^n + \Delta t (u^{(s)})_0^n$. Thus the fluid solution is computed on a rigid grid that moves with the interface. In 1-D with outflow boundary conditions on the right, this is trivial to implement as simple uniform rigid motion. However, in two or higher dimensions, or with more complex boundary conditions at the right of the fluid domain, a grid generation procedure would have to be used.

The stress and velocity interface conditions (2.3), (2.4) can be enforced in different ways. For example, setting the interface stress to the stress of the solid and the interface velocity to the velocity of the fluid,

$$u_{-1}^{(f)} = u_0^{(f)} \quad u_1^{(s)} = u_0^{(f)} \tag{2.5}$$

$$p_{-1} = -\sigma_0 \quad \sigma_1 = \sigma_0, \tag{2.6}$$

where the fluid velocity and solid stress are obtained by extrapolation from the interior. Other possibilities are to reverse the order of (2.5), (2.6) and set

$$u_{-1}^{(f)} = u_0^{(s)} \quad u_1^{(s)} = u_0^{(s)} \tag{2.7}$$

$$p_{-1} = p_0 \quad \sigma_1 = -p_0, \tag{2.8}$$

or to use an average of the above two conditions,

$$u_{-1}^{(f)} = (u_0^{(s)} + u_0^{(f)})/2 \quad u_1^{(s)} = (u_0^{(s)} + u_0^{(f)})/2 \tag{2.9}$$

$$p_{-1} = (p_0 - \sigma_0)/2 \quad \sigma_1 = (-p_0 + \sigma_0)/2. \tag{2.10}$$

A-priori, there is no reason to expect one condition to perform better than another, and all three conditions approximate (2.3), (2.4) with first order accuracy.

The Riemann problem with initial data

$$\rho^{(f)}(X,0) = 1 \quad u^{(f)}(X,0) = 0 \quad p(X,0) = 1 \quad X > 0$$

for the fluid, and

$$u^{(s)}(X,0) = 1 \quad \sigma(X,0) = -1 \quad X < 0$$

for the solid is used to demonstrate the performance of the different numerical interface conditions. The initial solid density, $\rho^{(s)}$, will be a problem parameter and we choose

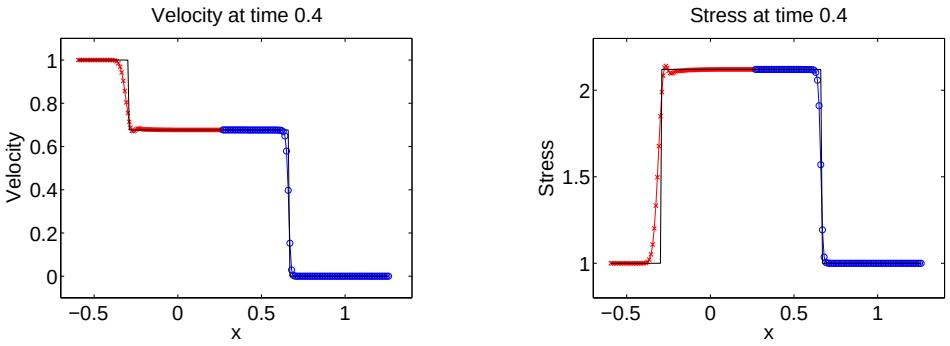

Figure 2: Solution of the Riemann problem showing velocity (left) and stress (right) as functions of the Eulerian (physical) coordinate x. Red x-symbols represent the solid, blue o-symbols the fluid, and the black line is the exact solution. The approximations use $N=100$ points in each domain.

Table 1: Behavior of interface conditions for different values of the initial density of the solid.

	$\rho^{(s)}$					
Interface conditions	0.005	0.04	0.125	2	20	50
(2.5),(2.6)	Stable	Stable	Stable	Stable	Unstable	Unstable
(2.7),(2.8)	Unstable	Unstable	Unstable	Stable	Stable	Stable
(2.9),(2.10)	Unstable	Stable	Stable	Stable	Stable	Unstable

$E=3\rho^{(s)}$ giving the wave speed $\sqrt{3}$ in the solid. Fig. 2 displays a representative numerical approximation as well as the exact solution at time 0.4. This example employs the numerical interface conditions of (2.7) and (2.8), CFL number 0.9, 100 grid points in each domain, and sets $\rho^{(s)}=2$. The solutions computed with (2.5), (2.6) or (2.9), (2.10) are similar (not shown). However, for larger or smaller values of $\rho^{(s)}$ some numerical interface conditions lead to unstable methods and the computed solution blows up. Notice here that because (2.1) becomes ill-posed for $p<0$, the computation is stopped when p becomes negative.

Table 1 summarizes the behavior of the three different numerical interface conditions for a few different values of $\rho^{(s)}$ with CFL 0.9. For these numerical experiments (2.5),(2.6) are unstable for large $\rho^{(s)}$ values, while (2.7), (2.8) are unstable for small $\rho^{(s)}$. The average condition (2.9), (2.10) combines, in some sense, the behavior of the two other conditions and is stable only when $\rho^{(s)}$ is not too small or too large. The first order Godunov method is usually thought to be very robust as a result of its significant numerical dissipation. Nevertheless, as Table 1 shows, when the density $\rho^{(s)}$ becomes very large or very small, the computation will break down for certain interface approximation techniques.

2.1 Linearization

In order to analyze the coupled problem, we linearize the systems (2.1) and (2.2). This technique is commonly used in numerical analysis of partial differential equations and is a

useful concept for a number of reasons. Firstly, instabilities are more clearly understood if they can be found in a linearized problem. In addition, most available mathematical tools only work for linearized problems, and stability of a linarized problem is often a necessary condition for stability of the full non-linear problem.

Before linearizing, we rewrite (2.1) with density, velocity, and pressure as dependent variables. The resulting system is

$$\begin{aligned} \rho_t+(u-s)\rho_x+\rho u_x&=0\\ u_t+(u-s)u_x+\frac{1}{\rho}p_x&=0\\ p_t+(u-s)p_x+\gamma p u_x&=0. \end{aligned} \tag{2.11}$$

We write the dependent variables (ρ,u,p) and the interface velocity s in (2.11) as the sum of a small perturbation ρ',u',p',s' and a linearization solution $\hat{\rho},\hat{u},\hat{p},\hat{s}$. Inserting this decomposition into (2.11), and neglecting all terms that are quadratic in the small perturbations gives the linearized system

$$\begin{aligned} \rho'_t+(\hat{u}-\hat{s})\rho'_x+\hat{\rho}u'_x+(u'-s')\hat{\rho}_x+\rho'\hat{u}_x&=0\\ u'_t+(\hat{u}-\hat{s})u'_x+\frac{1}{\hat{\rho}}p_x+(u'-s')\hat{u}_x-\frac{\rho'}{\hat{\rho}^2}\hat{p}_x&=0.\\ p'_t+(\hat{u}-\hat{s})p'_x+\gamma\hat{p}u_x+(u'-s')\hat{p}_x+\gamma p'\hat{u}_x&=0 \end{aligned}$$

Next, we obtain a constant coefficient problem by freezing the coefficients at a constant state that moves with the interface, i.e., $\hat{u}-\hat{s}=0$. For the constant coefficient problem, spatial derivatives of $\hat{\rho},\hat{u},\hat{p}$, and $\hat{s}$ are all zero and we arrive at the system

$$\begin{aligned} \rho'_t+\hat{\rho}u'_x&=0\\ u'_t+\frac{1}{\hat{\rho}}p'_x&=0\\ p'_t+\gamma\hat{p}u'_x&=0. \end{aligned} \tag{2.12}$$

The density is clearly decoupled from the velocity and pressure, and can be determined independently after (u',p') has been found. Therefore, we do not consider the density equation in the stability analysis that follows below. By dropping the prime on u and using the notation $\kappa^{(f)}=\gamma\hat{p}$ and $\sigma^{(f)}=p'$, we can write (2.12) as the wave equation

$$\begin{aligned} u_t^{(f)}+\frac{1}{\hat{\rho}^{(f)}}\sigma_x^{(f)}&=0\\ \sigma_t^{(f)}+\kappa^{(f)}u_x^{(f)}&=0. \end{aligned}$$

Notice that we have included a superscript (f) to clearly indicate the variables correspond to the fluid. Similarly, by denoting $\kappa^{(s)}=E$, the system in (2.2) is seen to be the wave

equation

$$u_t^{(s)} - \frac{1}{\rho^{(s)}}\sigma_x^{(s)} = 0$$
$$\sigma_t^{(s)} - \kappa^{(s)} u_x^{(s)} = 0.$$

Therefore, the fluid/structure problem (2.1), (2.2) can, to a first approximation (linearized, constant coefficients), be written as two coupled wave equations. As a result, the stability analysis to follow will consider two coupled wave equations. In section (4.1) we will demonstrate that the behavior predicted by this stability analysis is indeed present in numerical simulations of the full non-linear problem.

3 Analysis of interface conditions for the simple model

In order to understand the stability of various interface treatments, consider the problem of coupling two domains whose governing equations are linear elasticity with different densities and elastic parameters. Formally

$$\begin{bmatrix} u_L \\ \sigma_L \end{bmatrix}_t - \begin{bmatrix} \frac{\sigma_L}{\rho_L} \\ \kappa_L u_L \end{bmatrix}_x = \begin{bmatrix} u_L \\ \sigma_L \end{bmatrix}_t - \begin{bmatrix} 0 & \frac{1}{\rho_L} \\ \kappa_L & 0 \end{bmatrix} \begin{bmatrix} u_L \\ \sigma_L \end{bmatrix}_x = 0, \quad \text{for} \quad x < 0$$

$$\begin{bmatrix} u_R \\ \sigma_R \end{bmatrix}_t - \begin{bmatrix} \frac{\sigma_R}{\rho_R} \\ \kappa_R u_R \end{bmatrix}_x = \begin{bmatrix} u_R \\ \sigma_R \end{bmatrix}_t - \begin{bmatrix} 0 & \frac{1}{\rho_R} \\ \kappa_R & 0 \end{bmatrix} \begin{bmatrix} u_R \\ \sigma_R \end{bmatrix}_x = 0, \quad \text{for} \quad x > 0$$

and

$$\begin{aligned} u_L(0,t) &= u_R(0,t) \\ \sigma_L(0,t) &= \sigma_R(0,t). \end{aligned}$$

Here u_L, u_R, σ_L, and σ_R are functions of space and time and so the last equations are simply a statement that the velocities and stresses agree at the material interface $x = 0$. The quantities ρ_L, κ_L, ρ_R and κ_R are given constants. An analysis of the eigenstructure of the flux Jacobian of the governing equations reveals

$$\begin{bmatrix} 0 & \frac{1}{\rho_k} \\ \kappa_k & 0 \end{bmatrix} = R_k \Lambda_k R_k^{-1} = \begin{bmatrix} c_k & -c_k \\ \kappa_k & \kappa_k \end{bmatrix} \begin{bmatrix} -c_k & 0 \\ 0 & c_k \end{bmatrix} \begin{bmatrix} \frac{1}{2c_k} & \frac{1}{2\kappa_k} \\ -\frac{1}{2c_k} & \frac{1}{2\kappa_k} \end{bmatrix}$$

where the wave speed is $c_k = \sqrt{\kappa_k/\rho_k}$ and $k = L$ or R. For simplicity and clarity we make the assumption that $c = c_L = c_R$. This assumption can be relaxed, but at the cost of significantly increasing the complexity of the analysis with very little change in the result. Our interest is in analyzing various treatments of the interface conditions in the context of simple numerical methods and so we introduce the first order upwind interior

discretizations

$$\begin{aligned}\left[\begin{array}{c} u_k \\ \sigma_k \end{array}\right]_i^{n+1} = \left[\begin{array}{c} u_k \\ \sigma_k \end{array}\right]_i^{n} &- \frac{\Delta t}{\Delta x} R_k \Lambda_k^- R_k^{-1} \left(\left[\begin{array}{c} u_k \\ \sigma_k \end{array}\right]_{i+1}^{n} - \left[\begin{array}{c} u_k \\ \sigma_k \end{array}\right]_i^{n} \right) \\ &- \frac{\Delta t}{\Delta x} R_k \Lambda_k^+ R_k^{-1} \left(\left[\begin{array}{c} u_k \\ \sigma_k \end{array}\right]_i^{n} - \left[\begin{array}{c} u_k \\ \sigma_k \end{array}\right]_{i-1}^{n} \right)\end{aligned} \tag{3.1}$$

where

$$\Lambda_k^- = \left[\begin{array}{cc} -c & 0 \\ 0 & 0 \end{array}\right], \qquad \Lambda_k^+ = \left[\begin{array}{cc} 0 & 0 \\ 0 & c \end{array}\right].$$

These discretizations are stable under the CFL condition $\frac{c\Delta t}{\Delta x} \leq 1$ and we assume this constraint in the analysis to follow where applicable. The interior discretizations are applied on the computational domain $\hat{x}_i = \Delta x(i-1/2)$ for $i = \ldots,-1,0$ and $\tilde{x}_i = \Delta x(i+1/2)$ for $i = 0,1,\ldots$ to the left and right of the interface. The superscript n indicates the time step where $t_n = t_0 + n\Delta t$. The interface conditions are applied by making use of ghost cells whose centers are located at $\hat{x}_1$ and $\tilde{x}_{-1}$ (similar to Figure 1). In this way, the choice of interface conditions for any three point scheme, including the first order upwind scheme, boils down to a determination of $[u_L,\sigma_L]_1^n$ and $[u_R,\sigma_R]_{-1}^n$. For a first order implementation of the interface conditions it is sufficient to determine an interface velocity u_I^n and stress σ_I^n and use

$$\left[\begin{array}{c} u_L \\ \sigma_L \end{array}\right]_1^n = \left[\begin{array}{c} u_I \\ \sigma_I \end{array}\right]^n = \left[\begin{array}{c} u_R \\ \sigma_R \end{array}\right]_{-1}^n \tag{3.2}$$

to determine the unknown quantities in the ghost cells.

We will use a normal mode analysis [6] to investigate the stability properties of various interface treatments. Many of the steps of the proofs are common to all the methods and we describe those steps here. We seek solutions to the coupled discrete system (3.1) of the form

$$\left[\begin{array}{c} u_k \\ \sigma_k \end{array}\right]_i^n = z^n \left[\begin{array}{c} \tilde{u}_k \\ \tilde{\sigma}_k \end{array}\right]_i$$

where $\tilde{u}_{k,i}$ and $\tilde{\sigma}_{k,i}$ are bounded functions of space and z is a complex scalar. Denoting the characteristic normal modes by

$$\left[\begin{array}{c} a_k \\ b_k \end{array}\right] = R_k^{-1} \left[\begin{array}{c} \tilde{u}_k \\ \tilde{\sigma}_k \end{array}\right] \tag{3.3}$$

and using the interior discretization from (3.1) we find

$$z \left[\begin{array}{c} a_k \\ b_k \end{array}\right]_i = \left[\begin{array}{c} a_k \\ b_k \end{array}\right]_i + \frac{c\Delta t}{\Delta x} \left[\begin{array}{c} a_{k,i+1} - a_{k,i} \\ b_{k,i-1} - b_{k,i} \end{array}\right]. \tag{3.4}$$

Using the assumption that $\tilde{u}_{k,i}$ and $\tilde{\sigma}_{k,i}$ are bounded functions of space, the normal mode solutions are found as

$$\left[\begin{array}{c} \tilde{u} \\ \tilde{\sigma} \end{array}\right]_{L,i} = \left[\begin{array}{c} c \\ \kappa_L \end{array}\right] r^{i-1} a_{L,1} \text{ for } i \leq 0 \tag{3.5}$$

$$\begin{bmatrix} \tilde{u} \\ \tilde{\sigma} \end{bmatrix}_{R,i} = \begin{bmatrix} -c \\ \kappa_R \end{bmatrix} r^{-(i+1)} b_{R,-1} \text{ for } i \geq 0 \tag{3.6}$$

where $r = \frac{z-1+\frac{c\Delta t}{\Delta x}}{\frac{c\Delta t}{\Delta x}}$. Note that $|z|>1$ implies $|r|>1$ under the CFL constraint $0<\frac{c\Delta t}{\Delta x}<1$. We will insert these solutions into the interface condition, and obtain a system of two equations for the two unknowns $a_{L,1}$ and $b_{R,-1}$. According to the Gustafsson, Kreiss, Sundstöm (GKS) normal mode stability theory [6], the approximation is stable if and only if no non-trivial solutions of this sytem exists for $|z|>1$ and if there are no non-trivial solutions for $|z|=1$ that are generalized eigenvalues, see [6] for details.

3.1 The traditional option

The most common interface condition found in the fluid structure literature sets the interface velocity to the solid velocity and the interface stress to the fluid stress. The current example investigates two domains of linear elasticity and so an equivalent condition sets the interface velocity to the velocity from the left and the interface stress to the stress from the right domain. Use the first order approximations $u_I^n = u_{L,0}^n$ and $\sigma_I^n = \sigma_{R,0}^n$. From equation (3.2) we then obtain $u_{L,1}^n = u_{L,0}^n$, $\sigma_{L,1}^n = \sigma_{R,0}^n$, $u_{R,-1}^n = u_{L,0}^n$, and $\sigma_{R,-1}^n = \sigma_{R,0}^n$.

Theorem 3.1. *Let the interior discretization be given by (3.1) and the interface conditions by (3.2) with*

$$\begin{bmatrix} u_I \\ \sigma_I \end{bmatrix}^n = \begin{bmatrix} u_L \\ \sigma_R \end{bmatrix}_0^n. \tag{3.7}$$

Then the discretization is stable for

$$\lambda = \frac{c\Delta t}{\Delta x} < \min\left(1, \frac{4}{1+\frac{\rho_L}{\rho_R}}\right).$$

Thus, for $\frac{\rho_L}{\rho_R}<3$, the discretization is stable under the standard CFL-limit $\lambda<1$. When $\frac{\rho_L}{\rho_R}>3$, the stable CFL-limit decreases with increasing density ratio and $\lambda \to 0$ when $\frac{\rho_L}{\rho_R} \to \infty$.

Proof. By definition (3.3)

$$\begin{aligned} a_{L,1} &= \frac{1}{2c}\tilde{u}_{L,1} + \frac{1}{2\kappa_L}\tilde{\sigma}_{L,1} \\ b_{R,-1} &= -\frac{1}{2c}\tilde{u}_{R,-1} + \frac{1}{2\kappa_R}\tilde{\sigma}_{R,-1}. \end{aligned} \tag{3.8}$$

The interface conditions (3.2) and (3.7), along with the normal mode solutions (3.5) and (3.6) give

$$\begin{aligned} a_{L,1} &= \frac{1}{2c}\tilde{u}_{L,0} + \frac{1}{2\kappa_L}\tilde{\sigma}_{R,0} &&= r^{-1}\frac{1}{2}a_{L,1} + \frac{\kappa_R}{2\kappa_L}r^{-1}b_{R,-1} \\ b_{R,-1} &= -\frac{1}{2c}\tilde{u}_{L,0} + \frac{1}{2\kappa_R}\tilde{\sigma}_{R,0} &&= -r^{-1}\frac{1}{2}a_{L,1} + \frac{1}{2}r^{-1}b_{R,-1}, \end{aligned} \tag{3.9}$$

and the system for $a_{L,1}$ and $b_{R,-1}$ becomes

$$\begin{bmatrix} 1-\frac{1}{2r} & -\frac{\kappa_R}{2r\kappa_L} \\ \frac{1}{2r} & 1-\frac{1}{2r} \end{bmatrix} \begin{bmatrix} a_{L,1} \\ b_{R,-1} \end{bmatrix} = \begin{bmatrix} 0 \\ 0 \end{bmatrix}.$$

Non-zero $a_{L,1}$ and $b_{R,-1}$ exist if the determinant is zero, i.e., if

$$\left(1-\frac{1}{2r}\right)^2 + \frac{\kappa_R}{4\kappa_L r^2} = 0,$$

which has solutions

$$r = \frac{1}{2} \pm \frac{i}{2}\sqrt{\frac{\kappa_L}{\kappa_R}}.$$

Substituting the definition of r we find

$$z = \pm\frac{ic\Delta t}{2\Delta x}\sqrt{\frac{\kappa_L}{\kappa_R}} + 1 - \frac{c\Delta t}{2\Delta x}$$

from which

$$|z|^2 = \frac{c^2\Delta t^2}{4\Delta x^2}\left(\frac{\kappa_L}{\kappa_R}+1\right) + 1 - \frac{c\Delta t}{\Delta x}. \tag{3.10}$$

Recall that we are seeking unstable normal modes with $|z|>1$ and so the interface treatment is unstable for $\frac{\kappa_L}{\kappa_R} > \frac{4\Delta x}{c\Delta t} - 1$. As a result of the assumption of uniform wave speeds this is equivalent to the constraint on the mass ratios $\frac{\rho_L}{\rho_R} > \frac{4\Delta x}{c\Delta t} - 1$. □

3.2 The implicit option

The instability discussed in Section 3.1 is well known in practice and one method used to avoid the instability is to move to an implicit treatment. Although this works in practice, the stability of the method is not immediately clear and so we perform a normal mode analysis much as was done in Section 3.1. In order to achieve an implicit method, we introduce the implicit upwind method

$$\begin{aligned} \begin{bmatrix} u_k \\ \sigma_k \end{bmatrix}_i^{n+1} = \begin{bmatrix} u_k \\ \sigma_k \end{bmatrix}_i^{n} & - \frac{\Delta t}{\Delta x} R_k \Lambda_k^- R_k^{-1} \left(\begin{bmatrix} u_k \\ \sigma_k \end{bmatrix}_{i+1}^{n+1} - \begin{bmatrix} u_k \\ \sigma_k \end{bmatrix}_i^{n+1} \right) \\ & - \frac{\Delta t}{\Delta x} R_k \Lambda_k^+ R_k^{-1} \left(\begin{bmatrix} u_k \\ \sigma_k \end{bmatrix}_i^{n+1} - \begin{bmatrix} u_k \\ \sigma_k \end{bmatrix}_{i-1}^{n+1} \right). \end{aligned} \tag{3.11}$$

We again seek normal mode solutions and similar reasoning leads to the normal mode solutions

$$\begin{bmatrix} \tilde{u} \\ \tilde{\sigma} \end{bmatrix}_{L,i} = \begin{bmatrix} c \\ \kappa_L \end{bmatrix} s^{i-1} a_{L,1} \text{ for } i \le 0 \tag{3.12}$$

$$\left[\begin{array}{c}\tilde{u}\\ \tilde{\sigma}\end{array}\right]_{R,i}=\left[\begin{array}{c}-c\\ \kappa_R\end{array}\right]s^{-(i+1)}b_{R,-1}\text{ for }i\geq 0 \tag{3.13}$$

where $s=\frac{z-1+\frac{c\Delta t}{\Delta x}}{\frac{zc\Delta t}{\Delta x}}=\frac{\Delta x}{c\Delta t}\left(1-\frac{1}{z}\right)+1$. Notice that $|z|>1$ implies $|s|>1$ for $\frac{c\Delta t}{\Delta x}>0$.

Theorem 3.2. *Let the interior discretization be given by (3.11) and the interface conditions by (3.2) with*

$$\left[\begin{array}{c}u_I\\ \sigma_I\end{array}\right]^{n+1}=\left[\begin{array}{c}u_L\\ \sigma_R\end{array}\right]_0^{n+1}. \tag{3.14}$$

The resulting discretization is stable for $\frac{c\Delta t}{\Delta x}>0$.

Proof. The analysis follows an identical path to that in the proof of Theorem 3.1 with r being replaced by s. We therefore arrive at the solution

$$s=\frac{1}{2}\pm\frac{i}{2}\sqrt{\frac{\kappa_L}{\kappa_R}}.$$

Substitution of the definition for s leads to

$$z=\frac{2}{2+\lambda(1\pm i\sqrt{\alpha})}=\frac{4-2\lambda(-1\pm i\sqrt{\alpha})}{4+2\lambda+\lambda^2(1+\alpha)} \tag{3.15}$$

where $\lambda=\frac{c\Delta t}{\Delta x}$ and $\alpha=\frac{\kappa_L}{\kappa_R}$. Simple algebra shows

$$|z|^2=\frac{(4+2\lambda)^2+4\lambda^2\alpha}{(4+2\lambda)^2+2\lambda^2(4+2\lambda)(1+\alpha)+\lambda^4(1+\alpha)^2}=\frac{D}{N}.$$

(Notice that both D and N are real with $D>0$, $N>0$). Any unstable modes will have $|z|^2>1$ which is equivalent to the condition $D>N$. This easily reduces to

$$2\alpha>(4+2\lambda)(1+\alpha)+\frac{\lambda^2}{2}(1+\alpha)^2$$

and subsequently to

$$\alpha^2\frac{\lambda^2}{2}+\alpha\left(2+2\lambda+\lambda^2\right)+4+2\lambda+\frac{\lambda^2}{2}<0. \tag{3.16}$$

Clearly (3.16) can never be true because $\lambda>0$ and $\alpha>0$ and so there are no roots with $|z|>1$ which completes the proof. □

3.3 A stable alternate

For strictly hyperbolic problems, such as the current example under consideration, an explicit treatment of the interface conditions which is stable whenever the interior discretizations are stable would be extremely advantageous. To motivate such a treatment

we investigate a "characteristic" interface condition. The coupling interface condition (3.2) is applied and gives two constraints on the four ghost values. The remaining two constraints are obtained by extrapolating the outgoing characteristic from each domain. Extrapolation of the outgoing characteristics at first order gives

$$\frac{1}{c}\left(u^n_{L,1}-u^n_{L,0}\right)=\frac{1}{\kappa_L}\left(\sigma^n_{L,1}-\sigma^n_{L,0}\right) \tag{3.17}$$

and

$$-\frac{1}{c}\left(u^n_{R,0}-u^n_{R,-1}\right)=\frac{1}{\kappa_R}\left(\sigma^n_{R,0}-\sigma^n_{R,-1}\right). \tag{3.18}$$

Using (3.2) to eliminate $u_{R,-1}$ from (3.18) gives

$$-\frac{1}{c}\left(u^n_{R,0}-u^n_{L,1}\right)=\frac{1}{\kappa_R}\left(\sigma^n_{R,0}-\sigma^n_{R,-1}\right). \tag{3.19}$$

Solving (3.17) for $u_{L,1}$ and substituting back into (3.19) yields the condition

$$\sigma^n_I=\frac{\epsilon_L\sigma^n_{L,0}+\epsilon_R\sigma^n_{R,0}+u^n_{R,0}-u^n_{L,0}}{\epsilon_L+\epsilon_R} \tag{3.20}$$

where $\epsilon_L=\frac{1}{c\rho_L}$ and $\epsilon_R=\frac{1}{c\rho_R}$. It is then trivial to determine the interface velocity

$$u^n_I=\frac{\epsilon_R u^n_{L,0}+\epsilon_L u^n_{R,0}+\epsilon_L\epsilon_R\left(\sigma^n_{R,0}-\sigma^n_{L,0}\right)}{\epsilon_L+\epsilon_R}. \tag{3.21}$$

Equations (3.20) and (3.21) represent a first order characteristic implementation of the interface conditions, but we move one step further. In the condition we analyze (and later show results from), the term $u^n_{R,0}-u^n_{L,0}$ from (3.20) and the term $\epsilon_L\epsilon_R\left(\sigma^n_{R,0}-\sigma^n_{L,0}\right)$ from (3.21) are dropped because they are approximations to the interface coupling conditions of no jump in stress or velocity. The analysis to follow concerns the condition after their elimination although it seems likely, and computational experiment verifies, that they could be kept if one desired.

Theorem 3.3. *Let the interior discretization be given by (3.1) and the interface conditions by (3.2) with*

$$\begin{bmatrix} u_I \\ \sigma_I \end{bmatrix}^n=\frac{1}{\epsilon_L+\epsilon_R}\begin{bmatrix} \epsilon_R u_L+\epsilon_L u_R \\ \epsilon_L\sigma_L+\epsilon_R\sigma_R \end{bmatrix}^n_0 \tag{3.22}$$

where $\epsilon_L=\frac{1}{c\rho_L}$ *and* $\epsilon_R=\frac{1}{c\rho_R}$. *The resulting discrete system is stable under the CFL condition* $0<\frac{c\Delta t}{\Delta x}\leq 1$ *independent of the density jump across the material interface.*

Proof. Much as before, the definition of $a_{L,1}$ and $b_{R,-1}$ along with the interface conditions (3.2) and (3.22) can be combined to give

$$\begin{aligned} a_{L,1} &= \frac{\epsilon_R\tilde{u}_{L,0}+\epsilon_L\tilde{u}_{R,0}}{2c(\epsilon_L+\epsilon_R)}+\frac{\epsilon_L\tilde{\sigma}_{L,1}+\epsilon_R\tilde{\sigma}_{R,0}}{2\kappa_L(\epsilon_L+\epsilon_R)} \\ b_{R,-1} &= -\frac{\epsilon_R\tilde{u}_{L,0}+\epsilon_L\tilde{u}_{R,0}}{2c(\epsilon_L+\epsilon_R)}+\frac{\epsilon_L\tilde{\sigma}_{L,0}+\epsilon_R\tilde{\sigma}_{R,0}}{2\kappa_R(\epsilon_L+\epsilon_R)}. \end{aligned} \tag{3.23}$$

Substitution of the normal mode solution (3.5) and (3.6), and some slight rearrangement then leads to

$$\begin{aligned} (\epsilon_L+\epsilon_R)a_{L,1} &= \frac{\epsilon_R a_{L,1}-\epsilon_L b_{R,-1}}{2r}+\frac{\epsilon_L\kappa_L a_{L,1}+\epsilon_R\kappa_R b_{R,-1}}{2\kappa_L r} \\ (\epsilon_L+\epsilon_R)b_{R,-1} &= -\frac{\epsilon_R a_{L,1}-\epsilon_L b_{R,-1}}{2r}+\frac{\epsilon_L\kappa_L a_{L,1}+\epsilon_R\kappa_R b_{R,-1}}{2\kappa_R r}. \end{aligned} \tag{3.24}$$

The system for $a_{L,1}$ and $b_{R,-1}$ can then be written as

$$\begin{bmatrix} (2r-1)(\epsilon_L+\epsilon_R) & \epsilon_L-\epsilon_R\frac{\kappa_R}{\kappa_L} \\ \epsilon_R-\epsilon_L\frac{\kappa_L}{\kappa_R} & (2r-1)(\epsilon_L+\epsilon_R) \end{bmatrix}\begin{bmatrix} a_{L,1} \\ b_{R,-1} \end{bmatrix}=\begin{bmatrix} 0 \\ 0 \end{bmatrix}.$$

Non-zero $a_{L,1}$ and $b_{R,-1}$ may exist when the determinant is zero, i.e., if

$$(2r-1)^2(\epsilon_L+\epsilon_R)^2-\left(\epsilon_L-\epsilon_R\frac{\kappa_R}{\kappa_L}\right)\left(\epsilon_R-\epsilon_L\frac{\kappa_L}{\kappa_R}\right)=0.$$

The last term in this equation is seen to be zero by substituting the definitions $\epsilon_L=\frac{c}{\kappa_L}$ and $\epsilon_R=\frac{c}{\kappa_R}$. The determinant condition then yields the solution $r=\frac{1}{2}$. Substituting back into the definition of r we find

$$z=1-\frac{c\Delta t}{2\Delta x}$$

from which it is clear that $|z|<1$ for $0<\frac{c\Delta t}{\Delta x}<4$. Recall that the interior discretizations are stable for $\frac{c\Delta t}{\Delta x}\leq 1$ and this completes the proof. □

An interesting note concerning the interface condition in Theorem 3.3 is that the extension of the analysis to the case of variable characteristic speeds $c_L\neq c_R$ is rather trivial. For this case the weights are defined as $\epsilon_L=\frac{1}{c_L\rho_L}$ and $\epsilon_R=\frac{1}{c_R\rho_R}$. Recall that $\lambda_L=\frac{c_L\Delta t}{\Delta x}$ and $\lambda_R=\frac{c_R\Delta t}{\Delta x}$. Define $r_L=\frac{z-1+\lambda_L}{\lambda_L}$ and $r_R=\frac{z-1+\lambda_R}{\lambda_R}$. The normal mode analysis yields $r_L=\frac{1}{2}$ or $r_R=\frac{1}{2}$ from whence

$$z=1-\lambda_L \qquad \text{or} \qquad z=1-\lambda_R.$$

It is then easy to verify that $|z|<1$ for $0<\max(\lambda_L,\lambda_R)\leq 1$.

3.4 Extensions to second order discretizations

Extension of the analysis to second order (or higher) discretizations is, in principle, straightforward. However, we have found the resulting recurrence relations, polynomials, and the eventual solutions to be quite complicated and difficult to deal with. In fact we have only been able to solve these systems for restricted cases and we now present some results.

In order to treat the interface conditions to second order we must modify the discrete interface conditions (3.2). A straightforward second order treatment uses

$$\frac{1}{2}\left(\begin{bmatrix} u_L \\ \sigma_L \end{bmatrix}_l^n + \begin{bmatrix} u_L \\ \sigma_L \end{bmatrix}_{1-l}^n\right) = \begin{bmatrix} u_I \\ \sigma_I \end{bmatrix}^n = \frac{1}{2}\left(\begin{bmatrix} u_R \\ \sigma_R \end{bmatrix}_{-l}^n + \begin{bmatrix} u_R \\ \sigma_R \end{bmatrix}_{l-1}^n\right). \tag{3.25}$$

where l takes values $1,\ldots,N_g$ and N_g is the number of ghost cells required by the interior discretization. Given values for the interface velocity and stress one can use (3.25) to solve for the unknown ghost quantities in both domains. At this point it is convenient to introduce some additional notation. Second order interface conditions will require second order approximations to the interface velocity and stress from each domain. For instance, a second order approximation to the interface velocity according to the left domain is

$$u_{I,L}^n = \frac{3}{2}u_{L,0}^n - \frac{1}{2}u_{L,-1}^n$$

while for the right domain is

$$u_{I,R}^n = \frac{3}{2}u_{R,0}^n - \frac{1}{2}u_{R,1}^n.$$

Similar formulas are used to determine $\sigma_{I,L}^n$ and $\sigma_{I,R}^n$.

Let us examine the stability properties of the traditional and the new interface conditions using the first order upwind method (3.1) and the second order interface conditions (3.25).

Theorem 3.4. *Let the interior discretization be given by (3.1) and the interface conditions by (3.25) with*

$$\begin{bmatrix} u_I \\ \sigma_I \end{bmatrix}^n = \begin{bmatrix} u_{I,L} \\ \sigma_{I,R} \end{bmatrix}^n. \tag{3.26}$$

Then the discretization is stable for

$$\lambda = \frac{c\Delta t}{\Delta x} < \min\left(1, \frac{3}{2} - \frac{\sqrt{2}}{4}\sqrt{\frac{-7+2\alpha+9\alpha^2+\sqrt{(49+81\alpha)(\alpha+1)^3}}{(\alpha+1)^2}}\right)$$

where $\alpha = \frac{\rho_L}{\rho_R}$. *Thus, for* $\frac{\rho_L}{\rho_R} < \frac{-8+2\sqrt{17}}{2} \approx 0.123$, *the discretization is stable under the standard CFL-limit* $\lambda < 1$. *When* $\frac{\rho_L}{\rho_R} > \frac{-8+2\sqrt{17}}{2}$, *the stable CFL-limit decreases with increasing density ratio and* $\lambda \to 0$ *when* $\frac{\rho_L}{\rho_R} \to \infty$. *This stability bound is shown graphically in Figure 3.*

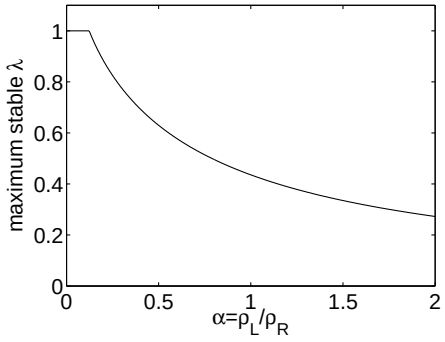

Figure 3: Stability bound for the second order interface condition with the first order upwind discretization. Shown is the maximum stable CFL number as a function of the mass ratio $\alpha = \frac{\rho_L}{\rho_R}$.

Proof. As in the proof of Theorem 3.1 we begin with the definition of $a_{L,1}$ and $b_{R,-1}$. Using the second order interface condition (3.25) and the definitions of the interface quantities in (3.26) we arrive at

$$\begin{aligned} a_{L,1} &= \frac{1}{2c}(2\tilde{u}_{L,0} - \tilde{u}_{L,-1}) + \frac{1}{2\kappa_L}(3\tilde{\sigma}_{R,0} - \tilde{\sigma}_{R,1} - \tilde{\sigma}_{L,0}) \\ b_{R,-1} &= \frac{1}{2c}(3\tilde{u}_{L,0} - \tilde{u}_{L,-1} - \tilde{u}_{R,0}) + \frac{1}{2\kappa_R}(2\tilde{\sigma}_{R,0} - \tilde{\sigma}_{R,1}). \end{aligned} \tag{3.27}$$

The normal mode solutions (3.5) and (3.6) are then used to give the system of equations for $a_{L,1}$ and $b_{R,-1}$

$$\begin{bmatrix} \frac{1}{2r} - \frac{1}{2r^2} - 1 & \frac{3\kappa_R}{2r\kappa_L} - \frac{\kappa_R}{2r^2\kappa_L} \\ \frac{3}{2r} - \frac{1}{2r^2} & 1 + \frac{1}{2r^2} - \frac{1}{2r} \end{bmatrix} \begin{bmatrix} a_{L,1} \\ b_{R,-1} \end{bmatrix} = \begin{bmatrix} 0 \\ 0 \end{bmatrix}. \tag{3.28}$$

The determinant condition leads to the equation

$$\left(2r^2 + 1 - r\right)^2 + \frac{\kappa_R}{\kappa_L}(3r-1)^2 = 0 \tag{3.29}$$

which has roots

$$r = \frac{1 + 3i\beta \pm \sqrt{-7 - 9\beta^2 - 2i\beta}}{4}, \qquad r = \frac{1 - 3i\beta \pm \sqrt{-7 - 9\beta^2 + 2i\beta}}{4} \tag{3.30}$$

where $\beta = \sqrt{\frac{\kappa_R}{\kappa_L}}$. By definition, $z = r\lambda - \lambda + 1$, where λ is the CFL number $c\Delta t/\Delta x$, and we must determine conditions when $|z| < 1$ (or equivalently $|z|^2 < 1$). Define f as the real part and g as the imaginary part of $\sqrt{-7 - 9\beta^2 \pm 2i\beta}$. It follows that f satisfies

$$f^4 + (7 + 9\beta^2) f^2 = \beta^2, \tag{3.31}$$

and consequently

$$f=\frac{1}{2}\sqrt{-14-18\beta^2+2\sqrt{49+130\beta^2+81\beta^4}},\qquad g=\frac{\pm\beta}{f}.$$

The four roots (3.30) consist of two complex conjugate pairs. Because $|z|$ does not depend on the sign of the imaginary part of r, there are only two cases to consider. These are

$$r=\frac{1}{4}\left(1\pm f+i\left(3\beta\mp\frac{\beta}{f}\right)\right).$$

From here it is straightforward to see

$$|z|^2=\left(-\frac{3\lambda}{4}\pm\frac{\lambda f}{4}+1\right)^2+\left(\frac{3\lambda\beta}{4}\mp\frac{\lambda\beta}{4f}\right)^2. \tag{3.32}$$

By substitution of β in terms of f from (3.31), the condition $|z|^2>1$ is straightforwardly transformed into a polynomial relation in f and λ. The resulting condition is

$$(\lambda-3/2)(1-f^2)\pm 4f>0,$$

where we note that f is monotonically increasing with β, and satisfies $0<f<1/3$. Therefore, there are no roots with $|z|>1$ when

$$\lambda<3/2\mp\frac{4f}{1-f^2}.$$

Only the minus sign gives a restriction over the CFL condition of the interior scheme. Substitution of f in terms of β and further straightforward formula manipulations give the final condition

$$\lambda<\frac{3}{2}-\frac{\sqrt{2}}{4}\sqrt{\frac{-7+2\beta+9\beta^2+\sqrt{(49+81\beta)(\beta+1)^3}}{(\beta+1)^2}}$$

which completes the proof. □

We turn now to the stability properties of the new interface coupling technique implemented at second order but again restrict ourselves to the first order interior discretization.

Theorem 3.5. *Let the interior discretization be given by (3.1) and the interface conditions by (3.25) with*

$$\begin{bmatrix} u_I \\ \sigma_I \end{bmatrix}^n=\frac{1}{\epsilon_L+\epsilon_R}\begin{bmatrix} \epsilon_R u_{I,L}+\epsilon_L u_{I,R} \\ \epsilon_L\sigma_{I,L}+\epsilon_R\sigma_{I,R} \end{bmatrix}_0^n \tag{3.33}$$

where $\epsilon_L=\frac{1}{c\rho_L}$ *and* $\epsilon_R=\frac{1}{c\rho_R}$. *The resulting discrete system is stable under the CFL condition* $0<\frac{c\Delta t}{\Delta x}\leq 1$ *independent of the density jump across the material interface.*

Proof. The proof follows now familiar lines beginning with the definition of $a_{L,1}$ and $b_{R,-1}$. Using the second order interface condition (3.25) and the definitions of the interface quantities in (3.33) we arrive at the equations for $a_{L,1}$ and $b_{R,-1}$

$$\begin{bmatrix} \frac{r-1}{2r^2}-1 & 0 \\ 0 & \frac{r-1}{2r^2}-1 \end{bmatrix} \begin{bmatrix} a_{L,1} \\ b_{R,-1} \end{bmatrix} = \begin{bmatrix} 0 \\ 0 \end{bmatrix}. \tag{3.34}$$

The solution is found as

$$r = \frac{1 \pm i\sqrt{7}}{4}$$

from which it is trivial to show that $|z| < 1$ for $0 < \lambda \leq 1$. □

Note that much as the case for Theorem 3.3, the stability of the interface condition in Theorem 3.5 for $c_L \neq c_R$ is easy to analyze. As before, the roots of the determinant condition separate and one obtains $r_L = \frac{1 \pm i\sqrt{7}}{4}$ or $r_R = \frac{1 \pm i\sqrt{7}}{4}$. Thus

$$|z|^2 = 1 + \lambda_L \left(\lambda_L - \frac{3}{2} \right) \qquad \text{or} \qquad |z|^2 = 1 + \lambda_R \left(\lambda_R - \frac{3}{2} \right).$$

In either case it is clear that $|z| < 1$ for $0 < \max(\lambda_L, \lambda_R) \leq 1$.

We make a few additional observations concerning the stability of the second order implementation of the interface conditions. Although we have used the first order upwind interior discretization, the analysis is directly applicable to higher order interior discretizations in certain limiting conditions. Take for instance the case when $\lambda = 1$. Here the first order discretization is exact as are many second order space-time coupled schemes. As a result, the analysis we have presented is applicable in this limit. As one relaxes from $\lambda = 1$, to $\lambda = 0.9$ for instance, the effect is an increase in numerical dissipation. As a result the bound for $\lambda = 1$ is a worst case. The quantitative decay from that bound will obviously vary depending on the interior discretization, but the qualitative behavior will remain unchanged. On the other hand, for $\lambda < 1$ it is common that the move from first to second order interior discretizations has the effect of reducing numerical dissipation. For such cases the limits for the first order interior discretization with the second order interface condition provides a best case bound. That is to say that if a density ratio is unstable with a first order interior discretization we expect it will be unstable with a similar second order interior discretization, however, if it is stable with the first order scheme it may be unstable as one moves to a second order scheme.

One final observation concerns density ratios near 1. Our analysis shows that one sided interface conditions, that is using stress from one side and velocity from the other, introduces possible stability limitations. Use of our new technique enables the stability constraints to be lifted. However, instead of implementing the new interface condition, one could argue that it would be simpler to instead determine which side has the denser material and apply the appropriate one sided conditions based on that test. The analysis of the

second order conditions shows that this will not always eliminate the stability constraints introduced as a result of the one sided approach. Take for instance the ratio $\frac{\rho_L}{\rho_R}=1$. The stability constraint of the one sided approximations at second order (Theorem 3.5) gives a maximum time step with $\lambda\approx 0.4397$ regardless of which side donates stress and velocity. In fact, for the second order one sided interface conditions, a time step restriction exists for $\frac{\rho_L}{\rho_R}\in(\frac{-8+2\sqrt{17}}{2},\frac{2}{-8+2\sqrt{17}})\approx(0.1231,8.123)$ regardless of which side donates the velocity and stress. This is a fairly harsh restriction and is likely to be worse with higher order approximations of both the governing equations and interface conditions.

4 Numerical examples

We demonstrate the practical implications of our stability analysis using a number of numerical experiments. To produce a problem with known exact solution we use the method of characteristics [7]. Because the model problem is linear with uniform wave speed, the characteristics are straight lines whose slopes are the wave speed. For the 1-D problem under consideration each point (x,t) is intersected by two characteristic curves each carrying information about the solution at that point. The characteristic equations tell us that

$$\frac{u}{2c}+\frac{\sigma}{2\kappa}=\text{constant} \quad \text{for} \quad \frac{x}{t}=-c \tag{4.1}$$

and

$$-\frac{u}{2c}+\frac{\sigma}{2\kappa}=\text{constant} \quad \text{for} \quad \frac{x}{t}=c. \tag{4.2}$$

To simplify the construction we assume that the initial condition has $\frac{u}{2c}+\frac{\sigma}{2\kappa}=0$ and $-\frac{u}{2c}+\frac{\sigma}{2\kappa}=f(x)$ which implies that the initial conditions set $u(x,0)=-cf(x)$ and $\sigma(x,0)=\kappa f(x)$. The solution at the interface ($x=0$) is easily determined as

$$\begin{aligned} u(0,t) &= \frac{-2cf(-ct)}{1+\frac{\kappa_R}{\kappa_L}} \\ \sigma(0,t) &= \frac{2f(-ct)}{\frac{1}{\kappa_R}+\frac{1}{\kappa_L}}. \end{aligned} \tag{4.3}$$

Using equations (4.1) and (4.2), the initial conditions, and the solution at the interface (4.3), the solution for any point (x,t) away from the interface can be found as

$$u(x,t)=\begin{cases} -cf(-ct) & \text{for} \quad x<-ct \\ \left(2f(-ct)+\dfrac{u(0,t_I)}{c}+\dfrac{\sigma(0,t_I)}{\kappa_L}\right)\dfrac{c}{2} & \text{for} \quad -ct\le x<0 \\ \left(\dfrac{u(0,t_I)}{c}-\dfrac{\sigma(0,t_I)}{\kappa_R}\right)\dfrac{c}{2} & \text{for} \quad 0\le x<ct \\ 0 & \text{for} \quad x\ge ct \end{cases}$$

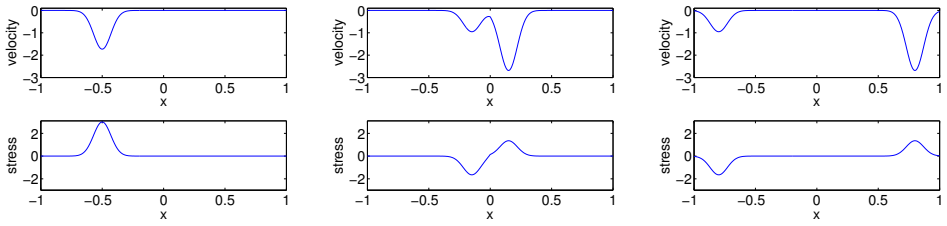

Figure 4: Exact solution to the test problem with $\frac{\rho_L}{\rho_R}=\frac{4\Delta x}{c\Delta t}-1$ at $t=0$ (left), $t=0.375$ (center), and $t=0.75$ (right).

and

$$\sigma(x,t)=\begin{cases}\kappa_L f(-ct) & \text{for} \quad x<-ct \\ \left(2f(-ct)+\dfrac{u(0,t_I)}{c}+\dfrac{\sigma(0,t_I)}{\kappa_L}\right)\dfrac{\kappa_L}{2} & \text{for} \quad -ct\le x<0 \\ \left(\dfrac{-u(0,t_I)}{c}+\dfrac{\sigma(0,t_I)}{\kappa_R}\right)\dfrac{\kappa_R}{2} & \text{for} \quad 0\le x<ct \\ 0 & \text{for} \quad x\ge ct\end{cases}$$

where $t_I=t-|x|/c$.

As a test case let the initial condition be given by $f(x)=e^{-100(x-\frac{1}{2})^2}$. The evolution of the exact solution is shown in Figure 4 with the representative density ratio $\frac{\rho_L}{\rho_R}=\frac{4\Delta x}{c\Delta t}-1$, $\frac{c\Delta t}{\Delta x}=0.9$, and $c=\sqrt{3}$. Initially we see the Gaussian pulse moving from left to right. At time $t=0.375$ the pulse is in the latter stages of interacting with the interface at $x=0$. Some portion of the wave pulse is transmitted through the interface and some portion is reflected. The final plot at $t=0.75$ is slightly before the reflected and transmitted pulses exit the domain to the left and right. We perform computations on the finite domain $x\in[-1,1]$ with the interface located at $x=0$. On the far left and far right boundaries, which are not considered in our analysis, we implement a first order characteristic non-reflecting boundary condition. At the interface we apply the appropriate interface condition for the given test case. Simulations are run using $\Delta x=1/50$ (51 grid cells in each domain), and a fixed CFL of $c\Delta t/\Delta x=0.9$. Time integration is carried out to the final time $t=5.0$ which is well after the pulses have left the domain.

Figure 5 shows the results when the traditional condition of Theorem 3.1 is used. In the figure, blue indicates the maximum error using the unstable density ratio $\frac{\rho_L}{\rho_R}=\frac{4\Delta x}{c\Delta t}-1+0.01$, and the red using the stable ratio $\frac{\rho_L}{\rho_R}=\frac{4\Delta x}{c\Delta t}-1-0.01$. The growth or decay rate for the admissible normal modes can be computed from (3.10) as $z\approx 1.001012$ and $z\approx 0.9989870$ respectively. The black lines in the figures are reference lines with those slopes and show the agreement of the simulation results to the theory.

The alternate interface condition of Theorem 3.3 is applied to the same problem and computational setup and the results plotted in Figure 6. The behavior for both density

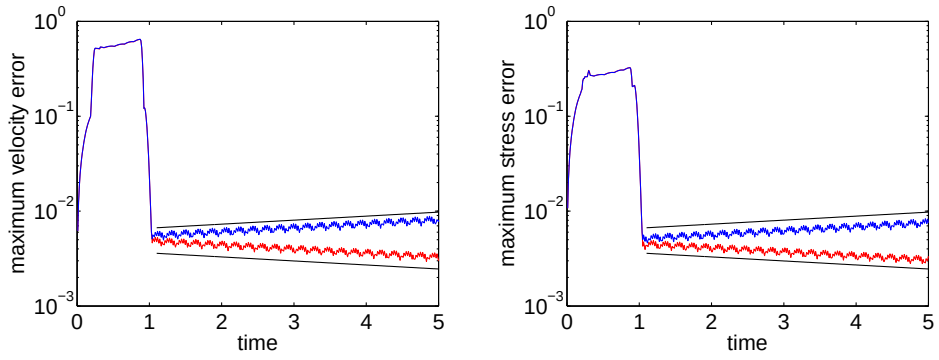

Figure 5: Errors in the velocity (left) and stress (right) using the traditional coupling technique of Theorem 3.1. In the plot the blue indicates the unstable density ratio $\frac{\rho_L}{\rho_R} = \frac{4\Delta x}{c\Delta t} - 1 + 0.01$, and the red the stable ratio $\frac{\rho_L}{\rho_R} = \frac{4\Delta x}{c\Delta t} - 1 - 0.01$. The black lines indicate the theoretical growth or decay rate of the admissible normal mode solutions.

ratios is remarkably similar and the stability of the scheme for either ratio is apparent.

In order to further demonstrate the efficacy of the condition in Theorem 3.3, the same Gaussian initial condition is used but now with the density ratios set to $\frac{\rho_L}{\rho_R} = 10^{10}$ and 10^{-10}. For the later, the traditional interface condition is stable and gives nearly identical results to the new interface condition. For the former the traditional scheme experiences rapid numerical blowup and by the second step the max error is already $\approx 10^8$. On the other hand, the new condition is stable for either ratio and produces roughly the same response for both cases. In fact the results for these extreme density ratios are roughly the same as the results found for the more modest ratios of Figures 5 and 6. Figure 7 shows these results.

We now move to numerical examples using the second order interface conditions. Figure 8 shows results obtained for the test problem with the first order interior discretization and the second order interface condition using both the traditional and new coupling techniques. For CFL $\lambda = 0.9$, the neutrally stable density ratio for the traditional technique is found to be $\frac{\rho_L}{\rho_R} \approx 0.1876$. We perform simulations on either side of this limit with $\frac{\rho_L}{\rho_R} = 0.1876 + 0.01$ chosen as an unstable case and $\frac{\rho_L}{\rho_R} = 0.1876 - 0.01$ as a stable case. The corresponding values for z are found to be approximately 0.9893 and 1.0104 respectively and the plot includes reference lines associated with those growth rates. The theoretical growth rates are shown to be well captured by the simulation. The same computations are carried out using the new coupling technique at second order and the results are as expected. The error decays rapidly after the pulse exits the computational domain. Note that the stress is not shown in either figure but the behavior is qualitatively similar to that of the velocity. Also note that the new coupling technique at second order gives qualitatively similar results for the larger density ratios $\frac{\rho_L}{\rho_R} = 10^{10}$ and $\frac{\rho_L}{\rho_R} = 10^{-10}$.

As a final test we use the same Gaussian initial condition but now implement a second

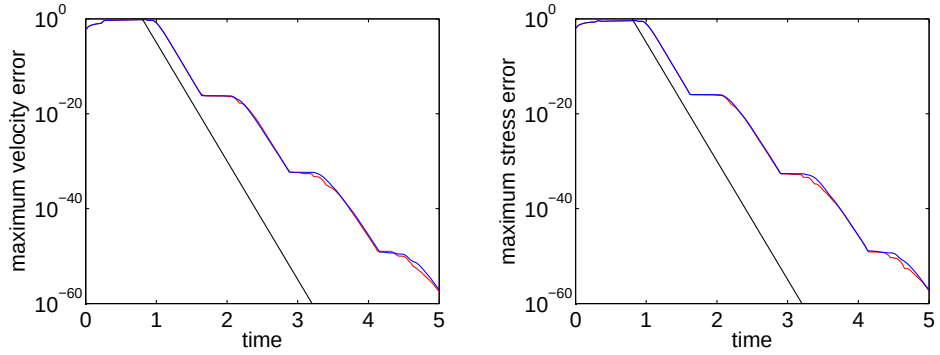

Figure 6: Errors in the velocity (left) and stress (right) using the new coupling technique of Theorem 3.3. In the plot the blue indicates the density ratio $\frac{\rho_L}{\rho_R} = \frac{4\Delta x}{c\Delta t} - 1 + 0.01$, and the red the ratio $\frac{\rho_L}{\rho_R} = \frac{4\Delta x}{c\Delta t} - 1 - 0.01$. The black lines indicate the theoretical decay rate of the admissible normal mode solutions.

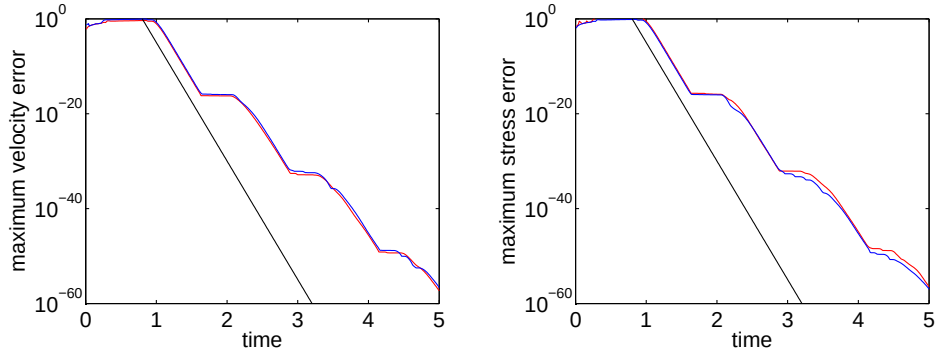

Figure 7: Errors in the velocity (left) and stress (right) using the new coupling technique of Theorem 3.3. In the plot the blue indicates the density ratio $\frac{\rho_L}{\rho_R} = 10^{10}$, and the red the ratio $\frac{\rho_L}{\rho_R} = 10^{-10}$. The black lines indicate the theoretical decay rate of the admissible normal mode solutions.

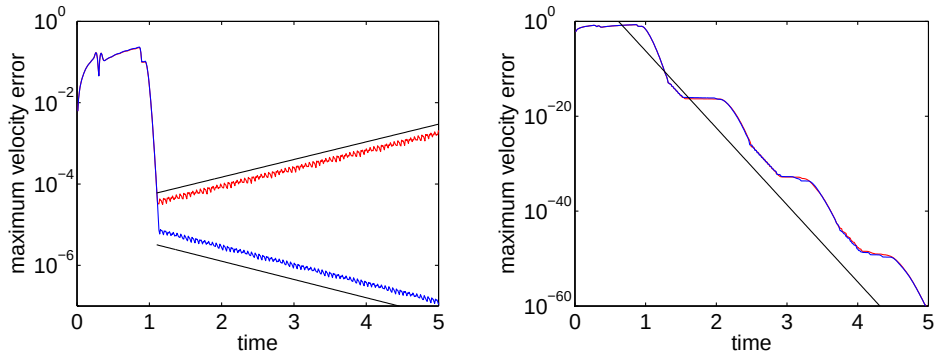

Figure 8: Errors in the velocity using the second order boundary conditions. On the left is the traditional option of Theorem 3.4, and on the right is our new coupling technique of Theorem 3.5. In the plot the blue indicates the density ratio $\frac{\rho_L}{\rho_R} = 0.1876 + 0.01$, and the red the ratio $\frac{\rho_L}{\rho_R} = 0.1876 - 0.01$. The black lines indicate the theoretical growth or decay rate of the admissible normal mode solutions. Note that the vertical scales differ between the two plots.

order upwind discretization along with the second order boundary condition to yield a fully second order scheme in both space and time. We no longer have a theoretical result in hand to indicate the stability limit and so instead we choose to illustrate the potential hazards via a convergence study. We use CFL λ=0.9 and $\frac{\rho_L}{\rho_R}$=0.25, and integrate in time to t_f=0.5. Figure 9 shows results for this convergence study. The maximum error in velocity is displayed as a function of time for the five resolutions $\Delta x = .02$, .01, .005, .0025, and .00125 for both the traditional interface treatment and the new proposed technique. For the traditional method the first resolution doubling gives reasonable results but upon the second doubling the instability begins to dominate the error. For the two finest resolutions the instability completely dominates the error. The unstable mode will also dominate the solution on the coarser grids if these computations are run longer in time. We can also notice that because instability growth depends on the number of time steps, the growth rate in physical time doubles as the time step is halved. For the new coupling technique, the instability is apparently not present and second order convergence is achieved at any fixed time. To demonstrate this fact, Figure 9 also presents a grid convergence study for the maximum velocity error at $t = 0.5$. Second order convergence in the maximum norm is demonstrated for the new coupling technique, and the convergence rate over the final grid doubling is calculated as 1.99. The traditional coupling technique shows rapid nonconvergence as the instability dominates. As a further test that the fully second order method with the new coupling condition is in fact stable, the simulation is allowed to run further in time so that the pulses leave the domain. As expected the errors decay off to $\approx 10^{-60}$ by $t = 5$ in much the same way as the previous results indicate. Furthermore, the behavior for the new coupling is unaltered for the large density jumps $\frac{\rho_L}{\rho_R} = 10^{-10}$ and 10^{10}.

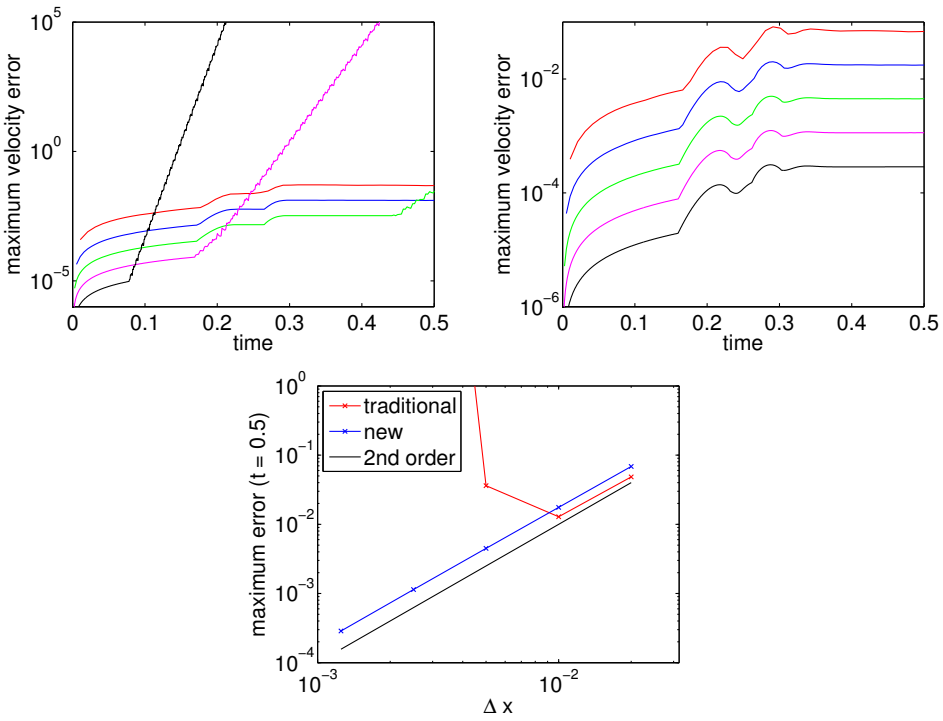

Figure 9: Errors in the velocity using a fully second order algorithm. At upper left are results using the traditional option of Theorem 3.4, while the top right shows our new coupling technique of Theorem 3.5. Here we use the fixed density ratio $\frac{\rho_L}{\rho_R} = 0.25$ and perform simulations at fixed CFL with the five resolutions $\Delta x = .02$ (red), $.01$ (blue), $.005$ (green), $.0025$ (magenta), and $.00125$ (black). The bottom plot shows the convergence of the error as $\Delta x \to 0$ at the fixed time 0.5 using both methods.

4.1 Introductory example with new interface condition

The analysis of the previous sections resulted in the interface condition (3.22), which is stable for the model problem, for all density ratios. It is here generalized and applied to the coupled Euler/linear elastic problem (2.1), (2.2) presented in Section 2.

The generalization of the stable interface condition (3.22) to the Euler/linear elastic problem is

$$u_{-1}^{(f)} = (\epsilon_s u_0^{(s)} + \epsilon_f u_1^{(0)})/(\epsilon_s + \epsilon_f) \quad u_1^{(s)} = (\epsilon_s u_0^{(s)} + \epsilon_f u_0^{(f)})/(\epsilon_s + \epsilon_f) \tag{4.4}$$

$$p_{-1} = (-\epsilon_s \sigma_0 + \epsilon_f p_0)/(\epsilon_s + \epsilon_f) \quad \sigma_1 = (\epsilon_s \sigma_0 - \epsilon_f p_0)/(\epsilon_s + \epsilon_f). \tag{4.5}$$

This condition is the same as (2.9), (2.10) but with weighted averages. The weights are generalized from (3.22) to be

$$\epsilon_s = 1/(\rho^{(s)} c_s) \quad \epsilon_f = 1/(\rho_I^{(f)} c_f)$$

where

$$c_s = \sqrt{E/\rho^{(s)}} \quad c_f = \sqrt{\gamma p_I / \rho_I^{(f)}}$$

and where first order extrapolation,

$$\rho_I^{(f)} = \rho_1^{(f)} \quad p_I = p_1$$

determines the interface values. The extrapolation is, of course, easy to generalize to higher orders of accuracy if needed. Notice that the continuous problem has no interface condition for the density of the fluid. In the numerical computation, we use extrapolation of the density to the ghost points for numerical boundary conditions.

Figures 10 and 11 show the computed solution of the Riemann problem in Section 2, computed in the same way as described there, but with the interface condition (4.4), (4.5). In Fig. 10, $\rho^{(s)}=0.001$, and in Fig. 11, $\rho^{(s)}=1000$. Both computations use CFL number 0.9 and are stable. Additional numerical experiments show that the new interface conditions lead to a method that is stable for CFL numbers up to 1 for arbitrary values of $\rho^{(s)}$. For example all cases investigate in Table 1 as well as the rather extreme cases of $\rho^{(s)} = 10^{\pm 10}$ are stable with (4.4), (4.5). Furthermore, extension of the new technique to second order in both space and time yields the same stability characteristics while the more traditional techniques suffer even more restrictive constraints than their first order counterparts.

5 Conclusions

In this paper we have discussed the stability of various discrete treatments of the interface coupling conditions for fluid-structure problems. The need to understand the stability properties of a given scheme was motivated by a numerical example which coupled an invicid and compressible ideal gas with a linearly elastic solid in 1-D. It was seen that some

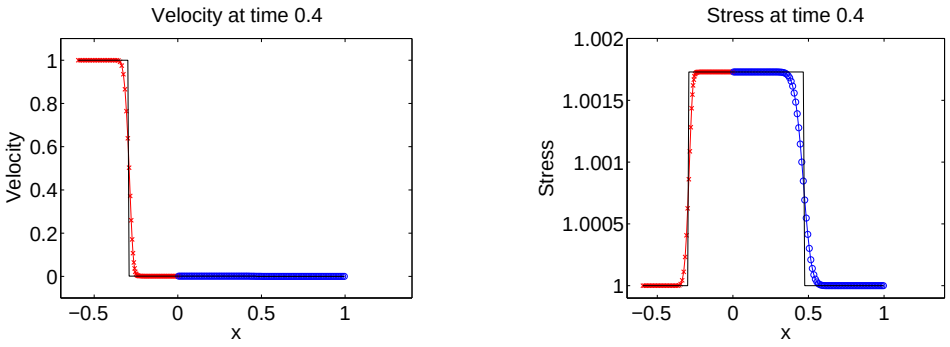

Figure 10: Solution of Riemann problem showing velocity (left) and stress (right) as functions of the Eulerian (physical) coordinate x. Red x-symbols represent the solid, blue o-symbols the fluid, and the black line is the exact solution. The approximations use $N = 100$ points in each domain and $\rho^{(s)} = 0.001$ with the new interface conditions.

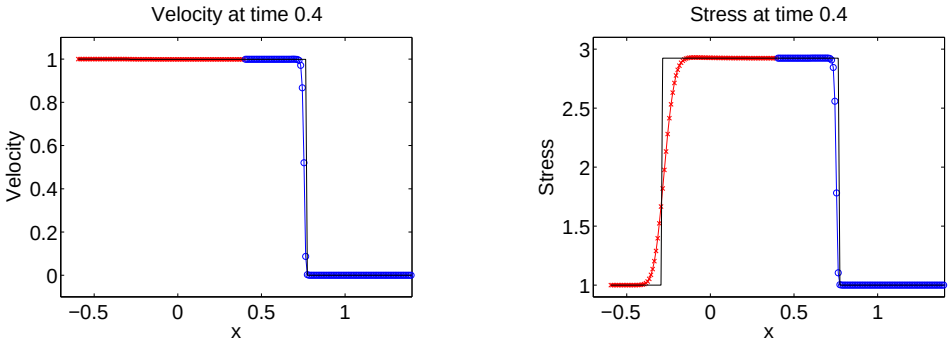

Figure 11: Solution of Riemann problem showing velocity (left) and stress (right) as functions of the Eulerian (physical) coordinate x. Red x-symbols represent the solid, blue o-symbols the fluid, and the black line is the exact solution. The approximations use $N = 100$ points in each domain and $\rho^{(s)} = 1000$ with the new interface conditions.

of the most natural discretizations are unstable as the ratio of densities becomes too large or too small. This problem was subsequently simplified to a coupling between two linearly elastic materials. A normal mode analysis showed the conditional stability of the simplest explicit treatment and the stability of an implicit treatment. A simplified characteristic interface condition was then derived and was proved to be stable up to the maximum stable CFL limit of the interior discretizations. We also extended the analysis to second order discretizations in certain limits and showed that the restriction on the traditional methods is even more severe with increasing order, but that the new condition remains stable for any density jump. A series of numerical examples explored these results and confirmed the conclusions. Finally the new coupling condition was applied to the original example and numerical examples demonstrated the stability of the resulting scheme for arbitrary jumps in density.

The specific results of this paper concern the stability of the fluid/structure interface for an invicid and compressible ideal gas with a linearly elastic solid, but the methods are much more widely applicable. For example, we have begun to pursue these techniques to investigate the numerical stability of interface treatments for the linearized Euler equations coupled with the equations of linear elasticity in two space dimensions, as well as the linearized Navier-Stokes equations with elastic and visco-elastic solids. For these cases, the solution to the Riemann problem can again be used to motivate coupling conditions, but more advanced analysis techniques may be required to prove stability. For instance it would be possible to use the same analysis technique as used here for the two dimensional problem with periodic boundary conditions in the second direction. Linearization and Fourier transformation of the second space dimension will lead to a problem of similar structure, but algebraically more involved, due to the dependence of the tangential Fourier mode. It is not clear whether a closed analytic condition for numerical stability would be obtained, but a detailed numerical investigation of the normal mode stability condition is certainly possible. Furthermore, the added possibility of surface waves traveling on the interface will make it interesting to also examine the stability of the interface in the continuous problem.

Acknowledgements
This study has been supported by Lawrence Livermore National Laboratory under the auspices of the U.S. Department of Energy through contract number DE-AC52-07NA27344.

References

[1] W. F. Noh, CEL: a time-dependent, two space dimensional, coupled Eulerian-Lagrange code, in: B. Alder, S. Fernbach, M. Rotenberg (Eds.), Methods in Computational Physics, Vol. 3, Academic Press, New York, 1964.
[2] R. P. Fedkiw, Coupling an Eulerian fluid calculation to a Lagrangian solid calculation with the ghost fluid method, J. Comput. Phys. 175 (2002) 200–224.
[3] R. Löhner, J. Cebral, C. Yang, J. D. Baum, E. Mestreau, C. Charman, D. Pelessone, Large-scale fluid-structure interaction simulations, Comput. Sci. Eng. 6 (2004) 27–37.

[4] R. Deiterding, R. Radovitzky, S. P. Mauch, L. Noels, J. C. Cummings, D. I. Meiron, A virtual test facility for the efficient simulation of solid material response under strong shock and detonation wave loading, Eng. Comput. 22 (2006) 325–344.
[5] R. J. LeVeque, Numerical Methods for Conservation Laws, Birkhauser, Basel, 1992.
[6] B. Gustafsson, H.-O. Kreiss, A. Sundström, Stability theory of difference approximations for mixed initial boundary value problems. II, Math. Comput. 26 (119) (1972) 649–686.
[7] G. B. Whitham, Linear and Nonlinear Waves, Wiley-Interscience, New York, 1974.